The onset of an eruption: selective assimilation of hydrothermal minerals during pre-eruptive magma ascent of the 2010 summit eruption of Eyjafjallajökull volcano (Iceland)

Pistolesi, M.[1], Cioni, R.[1], Francalanci, L.[1,2*], Bertagnini, A.[3], D'Oriano, C.[4], Braschi, E.[2] and Höskuldsson, A.[5]

[1] Dipartimento di Scienze della Terra, Università degli Studi di Firenze, via La Pira, 4, 50121, Firenze, Italy

[2] Istituto di Geoscienze e Georisorse, CNR, Sezione di Firenze, via La Pira, 4, 50121, Firenze, Italy

[3] Istituto Nazionale di Geofisica e Vulcanologia. Pisa, Italy

[4] Istituto Nazionale di Geofisica e Vulcanologia. Palermo, Italy

[5] Institute of Earth Sciences, University of Iceland, Reykjavik, Iceland

*Corresponding Author: Dipartimento di Scienze della Terra, Università di Firenze, via G. La Pira, 4, I-50121 - Firenze (Italy)

email: lorella.francalanci@unifi.it

Keywords: Selective assimilation; hydrothermal minerals; micro-Sr isotopes, opening phase, magma ascent dynamics.

Abstract

The complex processes occurring in the initial phases of an eruption are often recorded in the products of its opening stage, which are usually characterized by small volume and limited dispersal, and thus generally poorly studied. The 2010 eruption of Eyjafjallajökull (Iceland) represents a unique opportunity for these investigations thanks to the good preservation of tephra deposits within the ice/snow pack. A detailed geochemical investigation on the glassy groundmass of single ash clasts disclosed a population of fragments with unusual high $^{87}Sr/^{86}Sr$ (up to 0.70668) for Icelandic magmatism, and anomalous elemental composition with respect to most of the juvenile material of the eruption. This suggests that during its rise, before intruding into the ice cover, magma at a dyke tip selectively assimilated hydrothermal minerals with seawater-related, high-Sr isotopic ratios (zeolites, silica phases,

anhydrite) hosted in altered volcanic/epiclastic rocks. According to the observed precursory seismicity, only restricted to few hours before the onset of the eruption, this process could have accompanied subcritical aseismic fracture opening during the days before the eruption, possibly related to stress corrosion-cracking processes, which enhanced the partial dissolution/melting and subsequent selective assimilation of the host rocks.

Introduction

Studies of explosive eruptions are generally based on the products of their paroxysmal phases, recognised and correlated at the scale of the whole dispersal area (Nakamura, 1964; Thorarinsson, 1954; Booth et al., 1978; Fisher and Schmincke, 1984; Cas and Wright, 1987; Wilson, 1993; Cioni et al., 2015). Conversely, in most cases the very initial products of an eruption, often related to transient phases of weak intensity, are not studied in detail, as they are not easily recognized in the field due to the limited dispersal and to the fact that they are generally confined to very proximal sites, often not easily accessible. However, the information that might be derived from these products can be of fundamental importance to highlight timing and dynamics of the processes involved in the initial stages of magma ascent to the surface (Cioni et al., 2000; Cashman and Hoblitt, 2004; Meletlidis et al., 2012; Druitt, 2014). The study of initial deposits of an eruption can thus help the interpretation of its precursory signals, which mostly detected in the form of ground deformation or seismicity (e.g. Sparks, 2003; Dzurisin, 2007; Chouet and Matoza, 2013). These signals are related to pre-eruptive shallow magma storage and movements, involving the final fracturing of rocks beneath the eruptive vent and the associated decompressional path of magma to the surface. Consequently, a record of these processes can be preserved in the compositional and textural features of the first erupted material.

Here, a large dataset of the textural features and the glassy groundmass elemental/isotopic compositions of selected juvenile clasts is presented, in order to check possible micro-scale compositional heterogeneities within the products of the opening phase of the 2010 Eyjafjallajökull eruption (Iceland). The results are interpreted in terms of processes accompanying the initial phases of magma ascent and outbreak to the surface.

The 2010 eruption is particularly suitable for the investigation of its opening phase thanks to the perfect preservation of the deposits emplaced during the first part of the explosive event, which represent 3-4 hours of subglacial activity during which magma melted its way through the ice-filled summit caldera. The tephra clasts of this stage were packed within the snow/ice after emplacement and strongly contrast with those of the following ash-producing activity in terms of morphology and texture, as well as for their geochemical and isotopic signature.

1. The 2010 summit eruption: brief chronology of events

The 14 April - 22 May 2010 summit eruption of Eyjafjallajökull volcano (Iceland) was characterized by a large production of ash that was mainly dispersed towards the east and south-east; the ash cloud caused significant damage to vegetation and various economic sectors in Iceland, and reached the southern parts of Europe leading to the most dramatic global disruption of air traffic since the WWII (Miller, 2011; O'Regan, 2011). The climactic explosive activity was preceded (20 March-12 April) by a fissural basaltic eruption, characterized by lava fountains and lava flows located on the eastern flank of Eyjafjallajökull, outside of the caldera border. After 2 days of quiescence of seismic and eruptive activity, a summit eruption started on 14 April and continued, with variable intensity, for 39 days (Gudmundsson et al., 2012). Seismicity preceded by only few hours the onset of the summit eruption and was mainly concentrated in two main clusters at 1-2 km and 4-5 km, along a subvertical pipe below the summit (Tarasewicz et al., 2012). The 14 April - 22 May activity has been divided into three main phases (Gudmundsson et al., 2012; Bonadonna et al., 2013; Cioni et al., 2014):

- *Phase I*: A seismic swarm started at 22:29 UTC on 13 April, increasing in intensity during the following few hours. A subglacial eruption possibly started around 01:15 UTC of 14 April, marked by a gradual increase in low frequency tremor. The subglacial phase came to an end before 05:55 UTC, when a white, vapour-laden plume was observed above the summit (ICAO report, 2012). Activity during this "opening" stage likely started along a fissure several hundred meters long, as suggested by the alignment of at least 4 ice-melting cauldrons observed from the first airborne synthetic aperture radar images taken by the Icelandic Coast Guard (Magnusson et al., 2012). The intensity of the summit eruption gradually increased during the day, and culminated with the emergence at 18:30 UTC of a 9-10 km-high, dark ash-laden plume; the mass discharge rate reached about $1x10^6$ kg s^{-1} and the activity was characterized by steam-dominated and ash-poor plumes rising from a series of vents aligned along a 2 km-long, north-south oriented fissure. Flash floods (jökulhlaups) were immediately triggered, forcing the evacuation of around 800 people. Phase I was dominated by a continuous series of frequent (seconds to minutes) pulses, mainly driven by the interaction of the magma with the ice-melting water and ash slurry inside the caldera (Gudmundsson et al., 2012). This phase lasted until the early hours of 18 April, with more energetic pulses generating sustained ash plumes on 14, 16 and 17 April.

- *Phase II* of the eruption began on 18 April and was characterized by a significant drop in the intensity of explosive activity (mass discharge rate around $10^4 – 10^5$ kg s^{-1}), and by the onset of lava emission, which lasted until 4 May. With the exception of a strong explosive pulse on 28 April, low-level (typically below 5 km high),

ash-poor plumes characterized this phase. Seismic activity remained at prevalent shallow levels during Phase I and II, and volcanic tremor intensified in correspondence of the onset of lava effusion during Phase II.

- *Phase III*: intense explosive activity renewed from 5 May, generating large amounts of fine-grained tephra that were injected into the atmosphere up to 10 km above sea level and dispersed over Europe. During this phase seismic activity migrated downward up to 30 km depth, concentrating in some clusters aligned on a nearly vertical path under the volcano, suggesting the progressive involvement of magma stalling at depth (Tarasewicz et al., 2012). After 18 May, activity progressively declined, outlining the final part of the eruption which ended on 22 May 2010.

The total volume of tephra emitted during 39 days of activity has been estimated at 0.32 km^3 (0.19 km^3 DRE) and only about 5% of the volume reached the continental Europe; about 70% of material was produced during the first phase (0.27 km^3 or 0.15 km^3 DRE).

2. Tephra sampling and study methods

An extensive tephra sampling was carried out in the first days of May 2010, between 2 and 56 km from the vent, east and southeast of the volcano (see Bonadonna et al., 2011, Bagnato et al., 2013 and Cioni et al., 2014, for further sampling details). Tephra emplaced during Phase I was collected from the primary fallout deposits packed and interlayered in the ice (section EJ13, located ≈4.5 km east from the crater, Fig. 1). The basal layer (EJ13A) is a 2 cm-thick, coarse ash deposit; the intermediate tephra deposit (EJ13B) is a 5 cm-thick layer of coarse ash with scattered lapilli and the upper layer (EJ13C) is a fine-grained, 10 cm-thick, faintly stratified, ash deposit (Fig. 2). Sample EJ13A, in particular, was attributed to the opening stage of Phase I (14 April), whereas layers EJ13B and EJ13C to the peak of activity of Phase I (14-18 April), during which most of the tephra sequence was emplaced (Bonadonna et al., 2011, Cioni et al., 2014). Samples of Phase II (EJ13T and EJ07) were collected directly on the glacier, at 4.5 and 20 km from the vent, respectively. Tephra of Phase III was collected approximately 9 km east of the crater on May 5, while falling from the plume (EJ14T, EJ15). On the same day, scoria lapilli (EJ27) were also collected around the crater area.

Major and trace element contents and Sr isotope ratios of tephra were determined on whole-rock samples, on fresh matrix glasses of single juvenile ash clasts randomly collected in the 0.71-2 mm grain-size interval, and on plagioclase phenocrysts. Nd isotopes were analyzed on whole-rocks. Although our goal was the characterization of clasts from the opening stage (sample EJ13A), clasts collected from the following phases were also analysed in order to highlight the main differences among samples. In particular, in order to check possible magma

compositional heterogeneities at the micro-scale, Sr isotope analyses on single ash clasts (for a total of 24 analyses) from the different eruptive phases were performed collecting micro-samples of matrix glass by the *in-situ* microdrilling technique (Fig. 3). Using the same method, $^{87}Sr/^{86}Sr$ values were also determined *in-situ* on 1 mm-sized loose plagioclase phenocrysts (17 analyses) of different compositions (An_{12-84}) rimmed by juvenile glass, in order to check crystal/liquid isotopic equilibrium. Volatile contents in the groundmass of 6 obsidian ash clasts from EJ13A sample were measured by synchrotron Fourier Transform InfraRed (FTIR) microspectroscopy. Clasts used for microanalysis were accurately selected in order to study juvenile fragments characterized by fresh matrix glass and low microlite content; chemical analyses were always performed on glass portions far enough from phenocrysts and, as far as we could, microlites. Methods are reported in the Analytical Procedure section of the Supporting Information, together with Tables S1-S3 that summarize the complete dataset.

3. Morphology and textures of the juvenile ash clasts

The juvenile component ejected during the different phases of the eruption shows a large morphological and textural variability also at the scale of the single eruptive phase (Dellino et al., 2011; Cioni et al., 2014).

Four main clast types were identified in the juvenile ash fraction (Cioni et al., 2014): spongy finely vesicular (SFV), coarsely vesicular (CV), and fluidal (FL) clasts, characterized by moderate to high vesicularity, and blocky clasts (BL), showing incipient to moderate vesicularity and a glass-dominated groundmass (Fig. 2). The four types of clasts also differ by their internal texture (amount of microlites, amount and shape of vesicles; Cioni et al., 2014). Relative abundance of the different juvenile clasts varies between the studied samples: SFV, CV and FL clasts are usually dominant (>80 vol%), although with different proportions in the different phases, except only for the opening stage (sample EJ13A), where BL clasts reach 40 vol%. BL clasts are very rare in the following phases (Fig. 2). These are generally subequant, with 12-40 vol% of spherical to tubular vesicles, obsidian-luster appearance and very low crystallinity of the groundmass. Plagioclase, clinopyroxene and minor oxides represent the mineral groundmass phases, regardless of the texture and crystallinity of the clasts and of the eruption phase (Cioni et al., 2014).

4. Geochemistry of the juvenile ash clasts

Whole-rocks are mainly benmoreites, with some dacitic samples (Table S1) similar to the less alkaline glass compositions reported by Keiding and Sigmarsson (2012).

Matrix glasses have silica contents between 55 and 68 wt%, as also reported by recent works (Sigmarsson et al., 2011; Borisova et al., 2012; Gudmundsson et al., 2012; Keiding and Sigmarsson, 2012). There is no strong correlation between glass composition, clast type and stratigraphic position of the sample (Figs. 2, 4). Some clasts (mainly BL-type) from products of the opening stage (sample EJ13A), however, show anomalous compositions characterized by higher silica contents (up to 65.5 wt%) compared with those of Phase I (59-62.5 wt%; Fig. 4 and Table S2). Although major elements usually display good correlations with silica, these samples plot outside the general Al_2O_3 - SiO_2 negative correlation (Fig. 4c), having higher alumina contents. The same clasts also contain lower K_2O, MgO, V and Sc and higher Na_2O in respect with other glasses with comparable silica content from the successive eruptive phases (Fig. 4; Table S2).

Trace element contents of matrix glass are generally well inter-correlated and overlap the compositional trends of literature data (Sigmarsson et al., 2011; Borisova et al., 2012) (Fig. 4; Table S2), although Sigmarsson et al. (2011) report larger compositional variations (e.g., Th: 3.6-10.9 ppm, Rb: 26.0-80.5 ppm). Samples EJ13A and, to a lesser extent, EJ13B, show a larger scatter of Rb, Ba and U abundances than the other trace elements; U, in particular, is also more enriched in most of the clasts. BL clasts showing anomalous major element composition are also generally enriched in U, Rb and Ba (Fig. 4 and Table S2).

$^{87}Sr/^{86}Sr$ and $^{143}Nd/^{144}Nd$ of whole-rocks are virtually constant within the analytical errors (Fig. 5; Table S2); they are similar to those already reported for this eruption (Sigmarsson et al., 2011; Borisova et al., 2012) and fall in the typical isotope range of the Icelandic magmatism ($^{87}Sr/^{86}Sr$: 0.7026-0.7037; Sigmarsson et al., 2008) (Fig. 5). $^{87}Sr/^{86}Sr$ were also analyzed *in-situ* on matrix glasses of single clasts, selected based on different texture and composition. Results indicate that clasts from samples EJ13C and EJ15 have quite constant $^{87}Sr/^{86}Sr$ and similar to the whole-rock values; conversely, glasses from samples of the opening stage (EJ13A) and paroxysmal Phase I (EJ13B) show a larger Sr-isotopic variability, ranging from typical values recorded in Icelandic fresh volcanic products up to much higher values never found in Iceland magmatism (Fig. 5). Significantly, these high values are measured in the compositionally anomalous BL clasts of the opening stage, especially in the glass of clast D2 from sample EJ13A (hereafter *sample-[clast]*, e.g. EJ13A-[D2]) which attains a value of 0.70668, remarkably unusual for Icelandic magmatism. Considering that the blank contamination level during analyses resulted in negligible contribution (≤1%), and therefore not able to affect the third decimal digit of isotopic data (details in the Analytical Procedure section of the Supporting Information), the obtained high Sr isotope values have a real significance. Only one (EJ13B-[C6]) out of 5 clasts from the paroxysmal Phase I has $^{87}Sr/^{86}Sr$ significantly higher

than Icelandic isotopes (Fig. 5), although this clast, belonging to the finely vesicular group, is not characterized by anomalous elemental composition (Figs. 4, 5).

In-situ Sr-isotopes of plagioclase crystals with variable anorthite content are low, constant and similar to the whole-rock values (0.70324-0.70331), ranging from 0.70321 to 0.70335. A core-rim pair from a plagioclase with normal zoning and sieved core resulted in isotopic equilibrium (Fig. 5; Table S3), confirming that isotope ratios did not change during crystallization.

Groundmass glasses of six BL clasts from EJ13A have low water content in residual glasses, averaging at 0.54 wt% (0.35- 0.72 wt%); CO_2 content in these glasses was below the detection limit of the apparatus.

5. Discussion

Presented data point out some interesting characteristics of the juvenile ash clasts emitted during the opening stage of the 2010 Eyjafjallajökull summit eruption. These include:

- few clasts from the initial stage are characterized by high $^{87}Sr/^{86}Sr$ values and anomalous elemental compositions (higher SiO_2, Al_2O_3, Na_2O, U, Rb and lower MgO, K_2O) compared with the other products of the eruption;.
- the majority of clasts from the following phases of the eruption (irrespective of their textural features) have the typical isotopic compositions of Icelandic rocks ($^{87}Sr/^{86}Sr$: 0.7026-0.7037; Sigmarsson et al., 2008);
- most of the anomalous glass shards have similar textural features, being blocky, glassy, and nearly microlite-free fragments (BL type);
- differently from glass shards, plagioclase phenocrysts do not reveal any isotopic anomaly.

We interpret these characteristics as related to the processes occurring during magma ascent immediately preceding the onset of the eruption, and they are used to infer the modalities and relative timing of magma rise.

5.1. Anomalous compositions of the juvenile clasts from the opening stage

The remarkable unusual composition of some clasts from the opening stage can be interpreted as the result of the occurrence of transient, local-scale phenomena during the final ascent of the magma. The strongly anomalous isotopic composition measured in the BL clasts is particularly interesting. Firstly, we can exclude that the high Sr isotopes of these glass shards is related to assimilation of Icelandic fresh oceanic crust, due to the low $^{87}Sr/^{86}Sr$ that characterizes these rocks (Sigmarsson et al., 2008). As a consequence, the only way to increase radiogenic Sr content in magmas up to the measured values is to assimilate components derived by interaction with seawater strontium, having $^{87}Sr/^{86}Sr$ of 0.70920 (Elderfield and Greaves, 1981). These components could be represented by:

i) bulk oceanic crust altered by seawater circulation; ii) carbonate marine sediments; iii) alteration minerals formed by seawater-related hydrothermal fluids, where marine Sr can be particularly concentrated. Among the three options, we exclude the assimilation of sediments because, despite the high $^{87}Sr/^{86}Sr$ (e.g., Sveinbjörnsdottir et al., 1993), this cannot justify the elemental compositional variability observed in the anomalous clasts. Furthermore, with respect to the other products, these clasts do not show anomalous CaO contents (Table S2), as expected if assimilation of carbonate sediments had occurred.

In order to understand which component contaminated a part of the firstly erupted magma and to explain the $^{87}Sr/^{86}Sr$ and Sr contents of the anomalous glasses, we performed quantitative calculations, considering a process of simple contamination instead of assimilation + fractional crystallization (AFC) or any other more complex process involving crystallization. The exclusion of AFC or other processes is due to the low, Sr-isotope ratios measured in all the analysed plagioclase phenocrysts, which are also equal to those of most of the 2010 host magmas (Fig. 5; Tables S1-S3), and close to the average values measured for Icelandic magmas. Melt contamination without involvement of mineral phases clearly indicates that crystal fractionation was not contemporaneous with magma contamination. In particular, the two similar isotope ratios found in core and rim of a plagioclase phenocryst (Fig. 5; Table S3) suggest that phenocryst crystallization occurred separately from any assimilation process (in the opposite case, a higher Sr isotope in the rim would be expected).

Because the simple contamination process is described by mixing equation, we performed mixing calculation between low Sr-radiogenic magmas and components with seawater Sr-isotope ratios (Fig. 6a, b). The matrix glass of EJ13A-[D2] has high Sr-isotopes but relatively low Sr content compared with glasses of lower silica abundances (Fig. 6a); thus, the assimilated component leads to increase isotopes, without increasing Sr content. We can reasonably assume that the original Sr concentration in the uncontaminated magma was in the range measured for EJ13A glasses (190-367 ppm; Fig. 6a) and whole rock (359 ppm; Table S1). Accordingly, calculations indicate that, depending on the starting Sr content, the compositions of the EJ13A-[D2] and EJ13A-[b1+C1] clast can be achieved by high assimilation degrees (50-70 wt% and 15-55 wt%, respectively) of possible components with 185-260 ppm and 95-360 ppm of Sr, respectively (Fig. 6b). A mixing line (Sr contents of magma and contaminant: 210 and 240 ppm, respectively) fits both the EJ13A-[D2] and EJ13A-[b1+C1] compositions, indicating assimilation degrees of 55% and 20%, respectively. We suggest this is the most suitable model able to explain the shallow level magma contamination in the opening stage (Fig. 6b). It is noteworthy that the amount of assimilation would increase considering contaminants with Sr-isotopes lower than the seawater value.

These results allow excluding the seawater-altered bulk oceanic crust as possible contaminant, due to its $^{87}Sr/^{86}Sr$ much lower than 0.70920 (generally lower than 0.706, rarely reaching 0.707 even in palagonite; Menzies and Seyfried, 1976; Elderfield and Greaves, 1981; Staudigel and Hart, 1983; Kawahata et al., 2001) and also commonly lower than $^{87}Sr/^{86}Sr$ of the EJ13A-[D2] glass.

Selective assimilation of alteration minerals formed by seawater-derived hydrothermal fluids, where these minerals are the only crustal components melted by the hot magmas (Kitchen, 1985), seems therefore the most reasonable explanation for constraining the anomalous compositions of clasts erupted during the opening stage. Secondary mineral phases, possibly hosted in veins and vacuoles of the basaltic basement (e.g., Weisenberger and Selbekk, 2009), can allocate radiogenic Sr from seawater, attaining high Sr-isotopes up to the seawater values (e.g., Humphris and Bach, 2005; Marks et al., 2010). They also have specific compositions able to change the geochemical characteristics of the assimilating magmas towards those observed in the anomalous glasses. The assimilated minerals should account for the SiO_2, Al_2O_3, and Na_2O increase and the MgO, V and Sc decrease in the high $^{87}Sr/^{86}Sr$ glass shards, as well as the nearly constant (or negligible decrease) K_2O and CaO contents (Fig. 4; Table S2). The composition of the contaminating material (black boxes in figures 4a,c,e) has been tentatively quantified by inverse mixing calculation (Table S4 in the Electronic Supporting Information), using the hybrid composition of EJ13A-[D2] clast, the assimilation degree of 55 wt% resulted by the most suitable Sr vs $^{87}Sr/^{86}Sr$ model (Fig. 6b: mixing line with the contaminant at 240 ppm of Sr), and the most appropriate composition of assimilating magma deduced by geochemical trends of Figs. 4 and 6a. Specifically, the silica content of the latter magma has been approximately estimated from the Sr vs. SiO_2 negative correlation (Fig. 6a) fixing Sr content at 210 ppm (Fig. 6b); then, the other element contents have been assessed by their trends with silica (Fig. 4; Table S4). Among the variety of hydrothermal minerals (e.g., Alt et al., 1986; Jakobsson and Moore, 1986; Deer et al., 1992; Weisenberger and Selbekk, 2009), the association in different proportions of zeolites (mainly analcite for 38 wt% and phillipsite for 31 wt%, with 2% of chabasite), silica phases (24 wt%) and few amounts of apophyllite (5 wt%; Table S4) could be the most suitable assimilated mineral assemblage for explaining the previously calculated contaminant compositions of the EJ13A-[D2] clast glass (Table S4) (Marriner et al., 1990; Franzson et al., 2008; Weisenberger and Selbekk, 2009). We can also speculate that the similar Al_2O_3, SiO_2 and Na_2O contents and lower Sr isotopes of EJ13A-[b1+C1] and EJ13A-[C3] clast glasses (Figs. 4, 5), in respect with the EJ13A-[D2] clast glass, are linked to the expected compositional variability of the zeolite assemblage, both in elements and isotopes. These glasses could have indeed assimilated a lower amount of prevailing analcite + silica phases (having higher Al_2O_3, SiO_2 and Na_2O contents) or, more probable, a similar amount of an analogue zeolite

assemblage with lower $^{87}Sr/^{86}Sr$ (around 0.707) than seawater. In the latter case, the contamination degree and the assimilated hydrothermal mineral assemblage would remain the same for all the anomalous glasses but $^{87}Sr/^{86}Sr$ of the contaminant would not be constant at the seawater value as we could effectively expect. Hence, the elemental and isotopic compositions of the anomalous clasts can be reasonably achieved by selective assimilation of hydrothermal secondary components, justifying the deviations from the compositional trends of the other glasses (Figs. 4, 5).

Considering trace elements and their large variability in zeolites (e.g., Rb: 5-120 ppm, Ba: 40-2400 ppm; Wood et al., 1976; Deer et al., 1992; Pickhardt et al., 2000; Weisenberger and Selbekk, 2009), we can hypothesise the occurrence of assimilated minerals with particularly high Rb, Ba, U, and low Sr contents. This assumption is based on trace element contents of the EJ13A anomalous glasses, together with the scatter of U, Rb and Ba abundances in the products erupted at the beginning of the eruption (EJ13A and EJ13B; Figs. 2, 4).

Analyses carried out on tephra clasts from the overlaying stratigraphic layer of Phase I (sample EJ13B) show that only one clast (EJ13B-[C6]) has slightly higher $^{87}Sr/^{86}Sr$ than the isotopic variability of Icelandic rocks (Fig. 5). Glass from the same clast also shows a significantly different composition than those of the EJ13A-[D2] and EJ13A-[b1+C1] glasses, particularly containing higher Sr and lower silica and Na_2O contents. These evidences may suggest that a small amount of EJ13B magma, possibly less evolved than the assimilating EJ13A magma, was slightly contaminated by a different crustal component in respect to that involved in the EJ13A anomalous glasses. In Fig. 6b, a mixing model shows that the EJ13B-[C6] composition could be explained by only 4% assimilation of a possible component with quite high Sr abundances (900 ppm), starting from Sr content of the EJ13B whole rock (294 ppm). Based on these considerations, we may suppose this magma assimilated a different zeolite assemblage, possibly with also the involvement of anhydrite, having high Sr contents and Sr isotopes (Kawahata et al., 2001; Humphris and Bach, 2005; Rubio et al., 2005; Marks et al., 2010).

5.2. Significance of BL clasts

The textural features of BL clasts in the deposits of the opening stage of the eruption suggest mechanisms of hydromagmatic fragmentation (completely lacking in the following activity) and magma granulation by quenching, possibly occurred when magma firstly intruded at the base of the ice cover (Cioni et al., 2014). Accordingly, the low vesicularity of BL clasts and the absence of microlites also suggest that they possibly represent fragments of the sill/dyke body quenched at contact with ice (Magnusson et al., 2012; Cioni et al., 2014). Pressure at which quenching occurred can be derived from the dissolved water concentration measured in BL glass

(Tuffen et al., 2007; Stevenson et al., 2009; Tuffen et al., 2010). Using the solubility model of Papale et al. (2006) and a magma temperature of 1040°C (Keiding and Sigmarsson, 2012), results suggest that degassing stopped at pressures corresponding to an average water depth of 380 m (ice thickness: 414 m). This well agrees with the caldera glacier thickness (200-400 m; Magnusson et al., 2012) and indirectly suggests that, in the hypothesis that degassing was interrupted by ice-magma contact, the preceding syn-eruptive decompressional degassing occurred close to equilibrium (no water in excess). We suggest here that BL clasts are the product of non-explosive fragmentation of the vanguard magma intersecting the ice cover during the opening stage of the eruption, and erupted to the surface when the gas/water/pyroclast mixture broke its way through the summit glacier.

5.3. Magma ascent dynamics during the opening phase

The "typical Icelandic" values of Sr-isotopes of the analysed plagioclase phenocrysts, in strong disequilibrium with the values measured in the glass of anomalous BL clasts, suggest a late-stage contamination during magma ascent. This occurred after phenocryst crystallization and involved only a very small portion of the erupting magma, as suggested by the low amount of anomalous clasts (Figs. 4,5; Table S2). Given the occurrence of juvenile fragments with high Sr-isotopic values only in the deposits of the initial stage of the eruption, and the absence of isotopic equilibrium between this glass and phenocrysts, we propose that contamination involved only the vanguard portion of the ascending dyke while it opened its way to the surface (Fig. 7), after phenocryst crystallization.

Assimilation could have been favoured by the relatively low magma supply rate to the ascending dyke, which possibly characterized the precursory phases of the eruption, as previously supposed on the basis of syn-eruptive decompressional degassing probably occurring close to equilibrium. In this case, 1:1 proportions of magma to contaminant (i.e., up to 55% of assimilated crustal components) could be consistent with interaction between the head (and walls) of an opening dyke and the host rock. In this process, even assimilation of small amounts (compared to the entire volume of the erupted magma in the opening phase) of hydrothermal minerals hosted in the wallrock could have significantly contaminated the ascending magma, because only the small magma portion at the magma/wallrock contact of the dyke tip is involved in the process, without chemical re-equilibration with the inner and lower portions of the dyke which, in turn, continuously supplied the heat needed to assimilation (Fig. 7). These transient processes interesting only a small, well confined magma portion can be only detected when single clasts from the opening phase products are separately analysed.

To constrain the main physical parameters of this magma contamination process, we have roughly calculated the volume of contaminated magma and of related assimilated rocks, in order to hypothesize the volume balance between magma and assimilated material. A first order approximation for the total erupted material during the opening stage can be derived by the few available data on thickness of the EJ13A deposit, obtained tracing a nearly circular isopach for each available point (Fig. 1) and using the methods of Pyle (1989) and Legros (2000). The estimated deposit volume ($3.5x10^6$ m^3; average of the values from the two methods) can be converted to dense rock equivalent (DRE) of 1.2 $x10^6$ m^3, using a magma density of 2500 kgm^{-3} and an average deposit density of 900 kgm^{-3} (as measured in similar deposits; Williams, 1983; Coltelli et al., 1998), corresponding to a magma mass of $3.1x10^9$ kg (Table S5 in the Electronic Supporting Information). The low percentage of anomalous clasts, which are approximately 20% of the BL type clasts (Figs. 4,5; Table S2), and hence about 8% of the whole material erupted during the opening stage, suggests a mass of contaminated magma of $2.5x10^8$ kg (Table S5). This mass is used to constrain the volume of wallrock involved in the contamination process discussed above. An assimilation degree of 50 wt%, chosen among the highest values calculated by Sr-isotopic modelling, results in a mass of assimilated mineral paragenesis of about $1.3x10^8$ kg. In a selective assimilation, where only the alteration minerals are digested by the uprising magma (Kitchen, 1985), the volume of altered bulk rock involved in the contamination process depends by its degree of alteration (i.e., percentage of hydrothermal minerals), which can largely vary. In any case, using a moderate alteration degree of 20 wt% (e.g., Weisenberger and Selbekk, 2009) we estimate a mass of involved bulk rock of $6.3x10^8$ kg (corresponding to a volume of $3.1x10^5$ m^3 assuming a density of 2000 kg m^{-3} for an altered basement rock; Table S5) being aware of the fact that this estimation is largely conservative in the case of a more pervasively altered wallrock. Assuming that this mass was possibly confined in the contact zone with the dyke walls, we can calculate its thickness on the base of hypothesised dyke geometry. Direct observations of magma intercepting the glacier during the first stages of the eruption suggest a NNE-SSW oriented fissure a few hundred meters long, which possibly propagated from a maximum depth of 5 km (based on seismic data; Tarasewicz et al., 2012; Magnusson et al., 2012). Accordingly, confining the estimated volume of the bulk rock interested by selective assimilation along a dyke assumed to have a length between 50-200 m and depth between 1000-5000 m, we calculate a thickness of the shell of wallrock involved in the assimilation ranging from 0.15 to 3 m. This thickness represents a highly conservative estimation, as it could even be smaller in case of a more altered wallrock or of an assimilation degree lower than 50%, consistent with the modelling of intermediate Sr-isotope ratios such as those of EJ13A-[b1+C1] glasses (Fig. 6). Thus, these calculations indicate that the amount of assimilated material in the opening stage system is at least one order of magnitude lower respect to the

355 total erupted magma (Table S5), confirming a negligible thermal effect on magma. An independent confirmation
356 of an important interaction of the ascending magma with hydrothermally altered rocks derives from a study of the
357 ash erupted during the different phases of the eruption (Paque et al., 2016). Interestingly, the amount of zeolites
358 and minor smectites observed in the ash was greater during the first phase of the eruption and progressively
359 decreased during the following phases, possibly following the formation of a stable conduit system.
360 The abundant data on seismic activity preceding the beginning of the summit eruption can give some hints about
361 the timing of the assimilation event. Seismicity occurred only few hours before the onset of the summit eruption,
362 possibly related to the final fracturing of host rocks and consequent rapid magma ascent, and was mainly
363 concentrated in two main clusters at 1-2 km and 4-5 km along a subvertical pipe below the summit (Tarasewicz et
364 al., 2012). This time is probably too short for the opening and magma invasion of a dyke connecting the main
365 magma reservoir (4-5 km depth; Gudmundsson et al., 2012), suggesting that the upward migration of the dyke tip
366 from the main shallow reservoir around 4 km up to 1-2 km could have occurred aseismically at least in the two
367 days of seismic quiet separating the end of the lateral eruption and the onset of the summit eruption. A viable
368 mechanism for rock weakening and aseismic subcritical crack growth can be represented by stress corrosion, as
369 already recognized at other volcanoes (Anderson and Grew, 1977; Atkinsons, 1984; Kilburn and Voight, 1998;
370 Vinciguerra, 1999). This mechanism of chemical reaction between country rocks and fluids (possibly exsolving
371 magmatic fluids and geothermal fluids) is able to fracture rocks at stresses much smaller than their theoretical
372 strength. Stress corrosion has been considered as a possible mechanism generating intermediate to short-term
373 seismic quiescence or variation in seismic rate (Main and Meredith, 1991). Accordingly, at Eyjafjallajokull, the
374 process of selective assimilation of hydrothermal minerals by the vanguard magma could have started before the
375 seismic crisis that heralded the eruption; hot acidic fluids exsolved during pre-eruptive magma ascent might have
376 enhanced the selective dissolution of altered rocks, making available for magma contamination suitable portions of
377 melted/dissolved hydrothermal minerals through a complex process of fluid/melt interaction. The absence of
378 isotopic equilibrium between the small contaminated portion of the ascending magma and its phenocrysts,
379 however, confirms that the process of stress corrosion/assimilation possibly occurred on a short timescale (few
380 days?) , after phenocrysts crystallization; the days-long seismic quiescence which preceded the onset of the
381 summit eruption could so be considered an indirect measure of the minimum length of this time interval.
382

383 **6. Conclusive remarks**

Tephra clasts erupted during the very first (hours-lasting) phase of the 2010 Eyjafjallajökull eruption were immediately packed within the ice/snow cover and thus preserved after the eruption.

We performed microanalyses on matrix glass of single clasts from this opening phase; the obtained chemical dataset allowed to detect transient processes occurring during the final part of magma rise. In particular, results suggest that:

1) dense, obsidian, blocky clasts (BL) are abundant during the opening stage of Phase I; some of these (approximately 20%) show anomalous elemental compositions with respect to the material of the following phases of the eruption, as well as unusual high $^{87}Sr/^{86}Sr$ values, even for Icelandic magmatism;

2) based on quantitative mixing calculations, we propose that the very first erupted magma was contaminated by selective assimilation of hydrothermal minerals (e.g., zeolites, quartz, ±apophyllite, ±anhydrite) present in veins or vacuoles of basement rocks altered by seawater-derived fluids from which the high Sr-isotopes are derived;

3) this contamination occurred at shallow levels, during the slow ascent of a vanguard magma body in the pre-eruptive phase. Assimilation affected only a small portion of the ascending magma (possibly the magma hosted in the upward migrating tip of the intruding dyke), which, once reached the ice cover, rapidly quenched and fragmented to form BL clasts. These were finally ejected as soon a cauldron opened in the glacier and the eruptive column started, and were emplaced together with vesicular fragments in the basal deposit;

4) mechanisms of stress corrosion driven by exsolved acidic fluids at the tip of the migrating dyke could have enhanced the dissolution of shallow-level hydrothermal minerals of altered rocks and the final magma contamination. Such a process has been often discussed and reported as the possible cause of dyke propagation before an eruption. We suggest that the occurrence of magma contamination could represent an important side-effect of this important process, and that it should deserve more detailed studies in the future;

5) The presented data confirms the importance of studying in detail the products of the very initial phases of an eruption, as they can give important hints on the processes accompanying the final magma ascent and outbreak to the surface, giving information on timing and modalities of these processes.

Acknowledgements

M. Pistolesi, R. Cioni, L. Francalanci and A. Bertagnini were supported by the MIUR-PRIN Project “Asherupt” granted to R. Cioni. M. Ulivi is acknowledged for all the assistance during isotopic analyses. We also thank A. Perucchi for assisting C. D’Oriano during the analyses performed at the SISSI-Elettra beamline in Trieste. The

authors are grateful to C. Bonadonna, M. Rosi, M. Ripepe, R. Genco, D. Delle Donne, G. Lacanna, M. Hensch, and Þ. Sæmundsson for their contribution and discussion in the field.

References

Alt, J.C., Honnorez, J., Laverne, C., and Emmermann, R. (1986), Hydrothermal alteration of a 1km section through the upper oceanic crust, Deep Sea Drilling Project Hole 504B: mineralogy, chemistry and evolution of seawater–basalt interactions. J. Geophys. Res., 91, 10309–10335.

Anderson, O.L., and P.C. Grew (1977), Stress corrosion theory of crack propagation with applications to geophysics, Rev. Geoph. Space Science, 15(1), 77-104.

Atkinson, B.K. (1984), Subcritical crack growth in geological materials. J. Geophys Res., 89, 4077-4114.

Bagnato, E., A. Aiuppa, A. Bertagnini, C. Bonadonna, R. Cioni, M. Pistolesi, M. Pedone, and A. Hoskuldsson (2012), Scavenging of sulphur, halogens and trace metals by volcanic ash: The 2010 Eyjafjallajökull eruption, Geoch. Cosmoc. Acta, 103, 138-160, doi:10.1016/j.gca.2012.10.048.

Bonadonna, C., R. Genco, M. Gouhier, M. Pistolesi, R. Cioni, F. Alfano, A. Hoskuldsson, and M. Ripepe (2011), Tephra sedimentation during the 2010 Eyjafjallajökull eruption (Iceland) from deposit, radar, and satellite observations, J. Geophys. Res., 116(B12), doi:10.1029/2011JB008462.

Booth, B., R. Croasdale, G.P.L. Walker (1978), A quantitative study of five thousand years of volcanism on Sao Miguel, Azores. Philos. Trans. R. Soc. Lond., 288, 271-319.

Borisova, A. Y., J.-P. Toutain, A. Stefansson, S. Gouy, and P. de Parseval (2012), Processes controlling the 2010 Eyjafjallajökull explosive eruption, J. Geophys. Res., 117(B5), doi:10.1029/2012JB009213.

Cas, R.A.F., and J.V. Wright (1987). Volcanic succession: modern and ancient. Allen & Unwin, London, 472 pp.

Cashman, K.V., and R.P. Hoblitt (2004), Magmatic precursors to the 18 May 1980 eruption of Mount St. Helens, USA. Geology, 32, 141–144.

Chouet, B.A., and Matoza, R.S. (2013), A multi-decadal view of seismic methods for detecting precursors of magma movement and eruption. J. Volc. Geoth. Res. 252, 108–175.

Cioni, R., L. Gurioli, A. Sbrana, and G. Vougioukalakis (2000), Precursory phenomena and destructive events related to the Late Bronze Age Minoan (Thera, Greece) and AD 79 (Vesuvius, Italy) Plinian eruptions; inferences from the stratigraphy in the archaeological areas. Geol. Soc. London, Special Pub., 171, 123–141.

441 Cioni, R., M. Pistolesi, A. Bertagnini, C. Bonadonna, A. Hoskuldsson, and B. Scateni (2014), Insights into the
442 dynamics and evolution of the 2010 Eyjafjallajökull summit eruption (Iceland) provided by volcanic ash
443 textures, Earth and Planetary Science Letters, 394(C), 111–123, doi:10.1016/j.epsl.2014.02.051.
444 Cioni R., Pistolesi M., Rosi M. (2015). Plinian and subplinian eruptions. In „The encyclopedia of volcanoes“,
445 Sigurdsson, H., Houghton, B., McNutt, S., Rymer, H., & Stix, J. (Eds.). Elsevier: 519-536.
446 Coltelli, M., Del Carlo, P., Vezzoli, L. (1998). Discovery of a Plinian basaltic eruption of Roman age at Etna
447 volcano, Italy. Geology, 26(12), 1095-1098.
448 Deer W.A., R.A. Howie, and J. Zussman (1992), An introduction to the rock-forming minerals (2nd ed.).
449 Longman Scientific and Technical Group, Inc.
450 Dellino, P., M.T. Gudmundsson, G. Larsen, D. Mele, J.A. Stevenson, T. Thordarson, and B. Zimanowski (2012),
451 Ash from the Eyjafjallajökull eruption (Iceland): Fragmentation processes and aerodynamic behavior, J.
452 Geophys. Res., 117, doi:10.1029/2011JB008726.
453 Druitt, T.H. (2014), New insights into the initiation and venting of the Bronze-Age eruption of Santorini (Greece),
454 from component analysis, Bull. Volcanol., 76(2), doi:10.1007/s00445-014-0794-x.
455 Dzurisin D. (2007), Volcano Deformation. Geodetic Monitoring Techniques. Springer–Praxis Books in
456 Geophysical Sciences; 441 pp.
457 Elderfield H., and M. J. Greaves (1981), Strontium isotope geochemistry of Icelandic geothermal systems and
458 implications for sea water chemistry. Geoch. Cosmoch. Acta, 45, 2201-2212.
459 Fisher, R. V., and H. U. Schmincke (1984), Pyroclastic rocks. Springer, Berlin Heidelberg New York, 472 pp.
460 Franzson, H., Zierenberg, R., Shiffman, P., 2008. Chemical transport in geothermal systems in Iceland, evidence
461 from hydrothermal alteration. J. Volcanol. Geoth. Res. 173, 217-229.
462 Gudmundsson, M.T., T. Thordarson, A. Hoskuldsson, G. Larsen, H. Bjornsson, F.J. Prata, B. Oddsson, E.
463 Magnusson, T. Hognadottir, G. Petersen, C.L. Hayward, J.A. Stevenson, and I. Jonsdottir (2012), Ash
464 generation and distribution from the April-May 2010 eruption of Eyjafjallajökull, Iceland, Sci. Rep., 2,
465 doi:10.1038/srep00572.
466 Höskuldsson, Á. (2011), Eruption dynamics of the 2010 summit eruption at the Eyjafjallajökull volcano (Iceland):
467 Magma fragmentation, tephra stratigraphy and transport. Geophys. Res. Abstr. 13, EGU2011-14165.
468 Humphris, S.E., and W. Bach (2005) On the Sr isotope and REE compositions of anhydrites from the TAG
469 seafloor hydrothermal system. Geoch. Cosm. Acta, 69, 1511-1525.
470 International Civil Aviation Organization (ICAO) report, (2012). The 2010 Eyjafjallajökull eruption, Iceland.

471 Kawahata H., Nohara M., Ishizuka H., Hasebe S., Chiba H. (2001), J. Geoph. Res., 106, 11083-11099.
472 Keiding, J.K., and O. Sigmarsson (2012), Geothermobarometry of the 2010 Eyjafjallajökull eruption: New
473 constraints on Icelandic magma plumbing systems, J. Geophys. Res., 117, doi:10.1029/2011JB008829.
474 Kilburn, C.R.J., and B. Voight (1998), Slow rock fracture as eruption precursor at Soufriere Hills Volcano,
475 Montserrat, 1–4. Geophys. Res. Lett. 25, 3665–3668.
476 Kitchen, D.E., 1985. The partial melting of basalt and ist enclosed mineral-filled cavities at Scawt Hill, Co.
477 Antrim. Mineral. Magazin, 49, 655-662.
478 Jakobsson, S.P., and Moore, J.G. (1986), Hydrothermal minerals and alteration rates at Surtsey volcano, Iceland.
479 Geol. Soc. Am. Bull. 97, 648.
480 Legros, F. (2000). Minimum volume of a tephra fallout deposit estimated from a single isopach. Journal of
481 Volcanology and Geothermal Research, 96(1), 25-32.
482 Magnússon, E., M.T. Gudmundsson, M.J. Roberts, G. Sigurðsson, F. Höskuldsson, B. Oddsson (2012), Ice–
483 volcano interactions during the 2010 Eyjafjallajökull eruption, as revealed by airborne imaging radar. J.
484 Geophys. Res. 117 (B7), B07405.
485 Marks, N., P. Schiffman, R. Zierenberg, W.A. Elders, G.O. Friðleifsson, and H. Franzson. (2010), Isotopic
486 Evidence of Hydrothermal Exchange and Seawater Ingress from Alteration Minerals in the Reykjanes
487 Geothermal System: Results from the IDDP. Prooceedings World Geothermal Congress – Bali Indonesia.
488 Main, I. G. and P.G. Meredith (1991). Stress corrosion constitutive laws as a possible mechanism of intermediate-
489 term and short-term seismic quiescence. Geoph. J. Int. 107, 363–372.
490 Marriner G.F., Turney J., Langford J.I. (1990), Apophyllite group: effects of chemical substitutions on dehydration
491 behaviour, recrystallization products and cell parameters. Mineralogical Magazine, 54, 567-577.
492 Menzies, M., and W. E. Seyfried (1976), Basalt-seawater interaction: trace element and strontium isotopic
493 variations in experimentally altered glassy basalt. Earth Planet. Sci. Lett., 44(3), 463-472.
494 Meletlidis, S., A. Di Roberto, M. Pompilio, A. Bertagnini, I. Iribarren, A. Felpeto, P.A. Torres, and C. D'Oriano
495 (2012), Xenopumices from the 2011–2012 submarine eruption of El Hierro (Canary Islands, Spain):
496 Constraints on the plumbing system and magma ascent. Geophysical Res Lett., 39, L17302,
497 doi:10.1029/2012GL052675.
498 Miller, S.A. (2011), April 2010 UK Airspace closure: Experience and impact on the UK's air-travelling public and
499 implications for future travel. J. Air Transp. Manag. 17, 296–301.

500 Nakamura, K. (1964), Volcano-stratigraphic study of Oshima volcano, Izu.Bull. Eartquacke Res. Inst., 42, 649-
501 728.
502 O'Regan, M. (2011), On the Edge of Chaos: European Aviation and Disrupted Mobilities. Mobilities 6, 21–30.
503 Papale, P., R. Moretti, D. Barbato (2006), The compositional dependence of the saturation surface of H_2O + CO_2
504 fluids in silicate melts. Chem. Geol., 229, 78-95.
505 Paque, M., Detienne, M., Maters, E. C., Delmelle, P. (2016). Smectites and zeolites in ash from the 2010 summit
506 eruption of Eyjafjallajökull volcano, Iceland. Bulletin of Volcanology 1–10. doi:10.1007/s00445-016-1056-
507 x
508 Pickhardt, C., I.B. Brenner, J S. Becker, and H.J. Dietze (2000), Determination of trace elements in zeolites by
509 laser ablation ICP-MS Fresenius. J. Anal. Chem., 368, 79–87.
510 Pyle, D. M. (1989). The thickness, volume and grainsize of tephra fall deposits. Bulletin of Volcanology, 51(1), 1-
511 15.
512 Rosi, M. (1996), Quantitative reconstruction of recent volcanic activity: a contribution to forecasting of future
513 eruptions. In Monitoring and mitigation of volcano hazards, Springer Berlin Heidelberg, 631-674.
514 Rubio, M.A., P.R.L. Browne and C. Recio (2005), Clark Volcano dredged samples, Kermadec trench; Mineraly,
515 fluid inclusions and preliminary S-Isotope characterization. Proceed. World Geoth. Congress, Antalya,
516 Turkey, 24-29 April 2005, 1-10 pp.
517 Sigmarsson, O., I. Vlastelic, R. Andreasen, I. Bindeman, J.-L. Devidal, S. Moune, J.K. Keiding, G. Larsen, A.
518 Höskuldsson, and T. Thordarson (2011). Remobilization of silicic intrusion by mafic magmas during the
519 2010 Eyjafjallajökull eruption. Solid Earth, 2, 271-281.
520 Sigmarsson, O., J. Maclennan, and M. Carpentier (2008), Geochemistry of igneous rocks in Iceland: a review.
521 Jokull, 58, 139–160.
522 Sigmundsson, F., S. Hreinsdottir, A. Hooper, T. Arnadottir, R. Pedersen, M.J. Roberts, N. Oskarsson, A. Auriac, J.
523 Decriem, P. Einarsson, H. Geirsson, M. Hensch, B.G. O'feigsson, E. Sturkell, H. Sveinbjornsson, and K.L
524 Feigl (2010), Intrusion triggering of the 2010 Eyjafjallajökull explosive eruption, Nature, 468(7322), 426–
525 430.
526 Sparks, R.S.J. (2003), Forecasting volcanic eruptions. Earth Planet. Sci. Lett., 210, 1–15.
527 Staudigel, H., and S. Hart (1983), Alteration of basaltic glass: Mechanisms and significance for the oceanic crust-
528 seawater budget. Geoch. Cosmoch. Acta, 47(3), 337-350.

529 Stevenson, J.A., J.L. Smellie, D.W. McGarvie, J.S. Gilbert, and B.I. Cameron (2009), Subglacial intermediate
530 volcanism at Kerlingarfjöll, Iceland: Magma–water interactions beneath thick ice. J. Volc. Geoth. Res.,
531 185, 337–351.
532 Sveinbjörnsdóttir, Á.E., J. Eiríksson, Á. Geirsdóttir, J. Heinemeier, and N. Rud (1993), The Fossvogur marine
533 sediments in SW Iceland - confined to the Allerød/Younger Dryas transition by AMS 14 C dating. Boreas,
534 22, 147–157. doi:10.1111/j.1502-3885.1993.tb00174.x
535 Tarasewicz, J., B. Brandsdóttir, R.S. White, M. Hensch, and B. Thorbjarnardóttir (2012), Using microearthquakes
536 to track repeated magma intrusions beneath the Eyjafjallajökull stratovolcano, Iceland. J. Geophys. Res.
537 117, B00C06.
538
539 Thorarinsson, S. (1967), The tephra fall from Hekla on March 29th 1947 in Einarsson, T., Kjartansson, G. and
540 Thorarinsson, S. eds. The eruption of Hekla 1947-1948. Visindafelag Islendinga H.F. Leiftur, 3, 68
541 pp.Tuffen, H., D.W. McGarvie, and J.S. Gilbert (2007), Will subglacial rhyolite eruptions be explosive or
542 intrusive? Some insights from analytical models. Annals of Glaciology, 45, 87-94.
543 Tuffen, H., J. Owen, and J. Denton (2010), Magma degassing during subglacial eruptions and its use to reconstruct
544 palaeo-ice thicknesses. Earth-Science Reviews, 99(1-2), 1-18.
545 Vinciguerra, S. (1999), Seismic scaling exponents as a tool in detecting stress corrosion crack growth leading to
546 the September–October 1989 flank eruption at Mt. Etna Volcano. Geophys. Res. Lett. 26, 3685–3688.
547 Weisenberger, T., and R.S. Selbekk (2009), Multi-stage zeolite facies mineralization in the Hvalfjordur area,
548 Iceland. Int. J. Earth Sci. (Geol Rundsch), 98, 985–999.
549 Williams, S. N. (1983). Plinian airfall deposits of basaltic composition. Geology, 11(4), 211-214.
550 Wilson, C.J.N. (1993). Stratigraphy, chronology, styles and synamics of late Quaternary eruptions from Taupo
551 volcano, New Zealand. Philos. Trans. R. Soc. Lond., 343, 205-306.
552 Wood, D.A., I.L. Gibson, and R.N. Thompson (1976), Elemental mobility during zeolite facies metamorphism oft
553 he Tertiary basalts of Eastern Iceland. Contrib. Mineral. Petrol., 55, 241-254.
554
555 **Figure captions**
556
557 **Figure 1** - General map with sampling sites. Green dots refer to samples used in this study. Red diamonds
558 represent other surveyed sites during the fieldwork. Dispersal of the opening phase deposit is also shown with

559 hatched lines (thickness in cm). Geographic coordinates of sampling sites are: EJ13 UTM 27V 572791 7056448,
560 EJ13T UTM 27V 572791 7056448, EJ07 UTM 27V 588031 7051116, EJ14T UTM 27V 570354 705628, EJ15
561 UTM 27V 577553 7053608, EJ27 UTM 27V 566401 7057469.
562
563 **Figure 2** - Stratigraphic sequence packed within the ice with samples (EJ13A, EJ13B, EJ13C, EJ07, EJ15) and
564 relative abundances (vol.%) of different clast types within each sample (BL=blocky-obsidian clast; SFV=spongy
565 finely vesicular clast; CV=coarsely vesicular clast; FL=fluidal clast). Back-scattered electron microscopy images
566 of different clast types are also shown. The base of the sequence also shows tephra of basaltic lava fountains from
567 the effusive fissural eruption occurred on the East flank of Eyjafjallajökull volcano from 20 March to 12 April
568 2010. Please note that the picture of the tephra sequence do not correspond exactly to EJ13 location but was taken
569 ≈2 km eastwards, where also the basaltic layer was preserved (photo by A. Hoskuldsson; geographic coordinates
570 27V 576791 7057007 UTM).
571
572 **Figure 3** - Comparison between back-scattered electron microscopy images of clasts before (left) and after (right)
573 *in-situ* microdrilling.
574
575 **Figure 4** - Inter-elemental diagrams for matrix glass compositions of ash clasts from samples EJ13A and EJ13B,
576 reported according to their different morphology (BL=blocky-obsidian clast; CV=coarsely vesicular clast,
577 SFV=finely vesicular clast; *n.d.*=not determined). For comparison, glass compositions of EJ13C (Phase I) and
578 Phase II - III samples are also reported as variation field. Clast names show those with anomalous high Sr isotopes
579 (see Fig. 5). Crosses in figures b, d, f represent data reproducibility on trace elements as 2 standard deviations
580 from the mean. Lines in figures a, c, e show examples of mixing calculation between the assimilating magma (full
581 circles) and the contaminating material (boxes); the latter composition has been tentatively quantified by inverse
582 mixing calculation (Table S4 in the Electronic Supporting Information), using the hybrid composition of EJ13A-
583 [D2] clast explained by $^{87}Sr/^{86}Sr$ model (see Fig. 6) through an assimilation degree of 55 wt% (see text and Table
584 S4 for other explanations). The composition of the anomalous clast with higher silica content (down triangle),
585 where Sr isotopes and trace elements are not determined, is probably explained by increasing the quartz/zeolite
586 proportion in the assimilated material.
587

588 **Figure 5** - $^{87}Sr/^{86}Sr$ vs major element diagrams for matrix glasses of single clasts from the analyzed samples
589 (EJ13A, EJ13B, EJ13C for Phase I, EJ15 for Phase III). *In-situ* isotopes (glass and plagioclase) have been
590 analyzed by microdrilling technique. Error bars are inside the symbols. Some matrix glasses (e.g. b1+C1) from
591 distinct, but geochemically similar, clasts have been combined to achieve the micro-milled glass sufficient for
592 allowing Sr-isotope analyses.
593
594 **Figure 6** - Sr contents versus silica (a) and $^{87}Sr/^{86}Sr$ (b) diagrams for matrix glasses of single clasts. Symbols and
595 compositional field are as in Figures 4 (a) and 5 (b). Error bars are inside the symbols. The best fits of mixing
596 calculations are reported in figure (b) as mixing lines between uncontaminated magmas, having low Sr-isotopes
597 and different Sr contents, and assimilated hydrothermal minerals assumed to have $^{87}Sr/^{86}Sr$ of seawater (Elderfield
598 and Greaves, 1981). The variable Sr contents of the contaminating mineralogical paragenesis are calculated for
599 each assumed Sr abundance in the uncontaminated magmas, using for the latter the minimum (190 ppm) and
600 nearly maximum (350 ppm) values and the more suitable value (210 ppm) that better fits two clast glass
601 compositions. Transversal bars along the lines with numbers indicate contamination degrees (in %).
602
603 **Figure 7 -** Simplified sketch of selective assimilation of hydrothermal mineral paragenesis present in altered rocks
604 by the opening stage magma during its early ascent towards the surface. Minerals dissolution was possibly
605 enhanced by stress corrosion mechanism driven by exsolved acidic fluids at the tip of the migrating dyke. When
606 magma reached the ice cover rapidly quenched (to form blocky clasts) and assimilation stopped due to fast ascent.
607 *Legend* – Solid (1) and melted (2) hydrothermal minerals in veins and vacuoles; 3: release of exsolved acidic
608 fluids.

Figure 1

Click here to download high resolution image

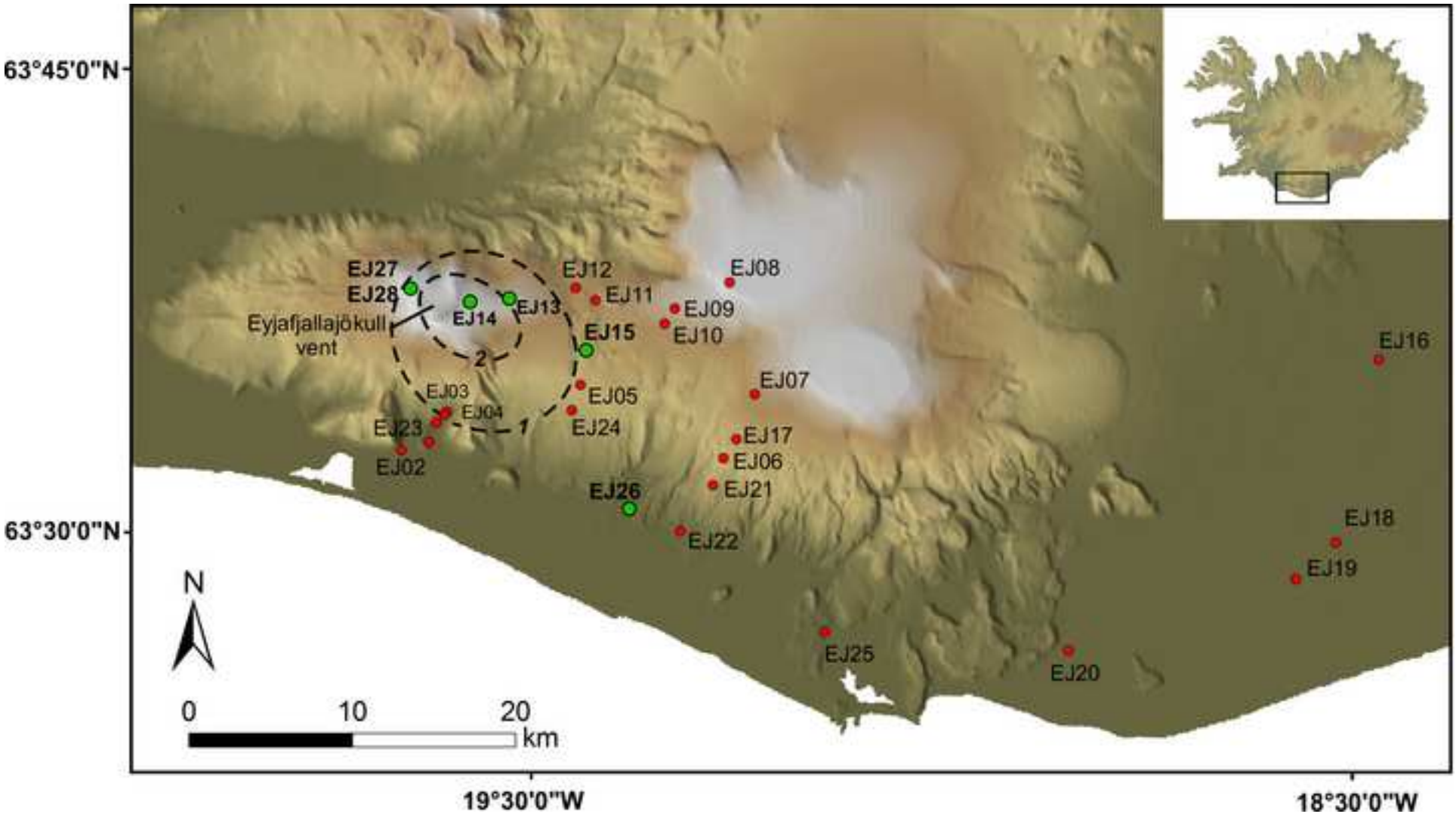

Figure 2

Click here to download high resolution image

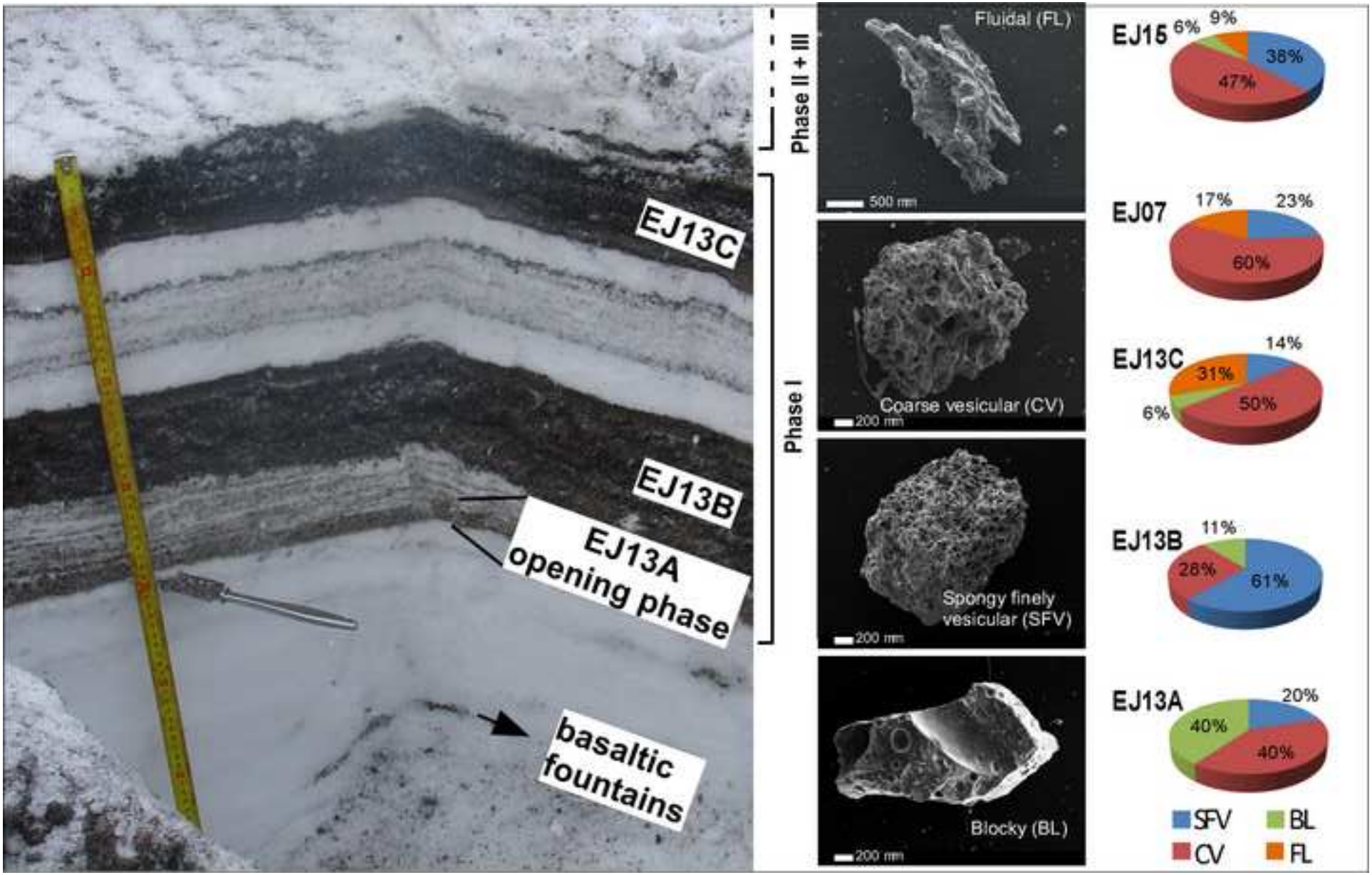

Figure 3

Click here to download high resolution image

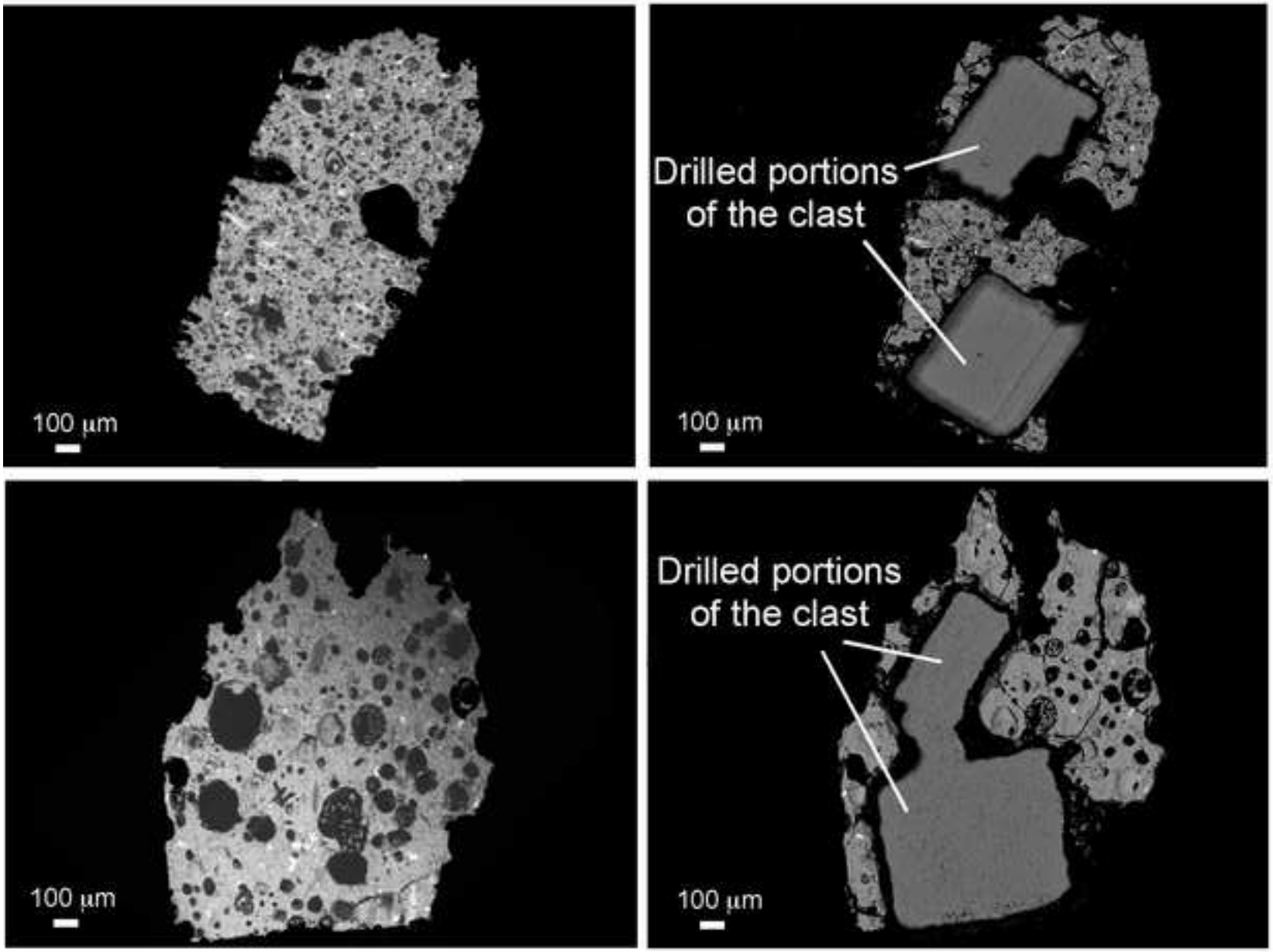

Figure 4

Click here to download high resolution image

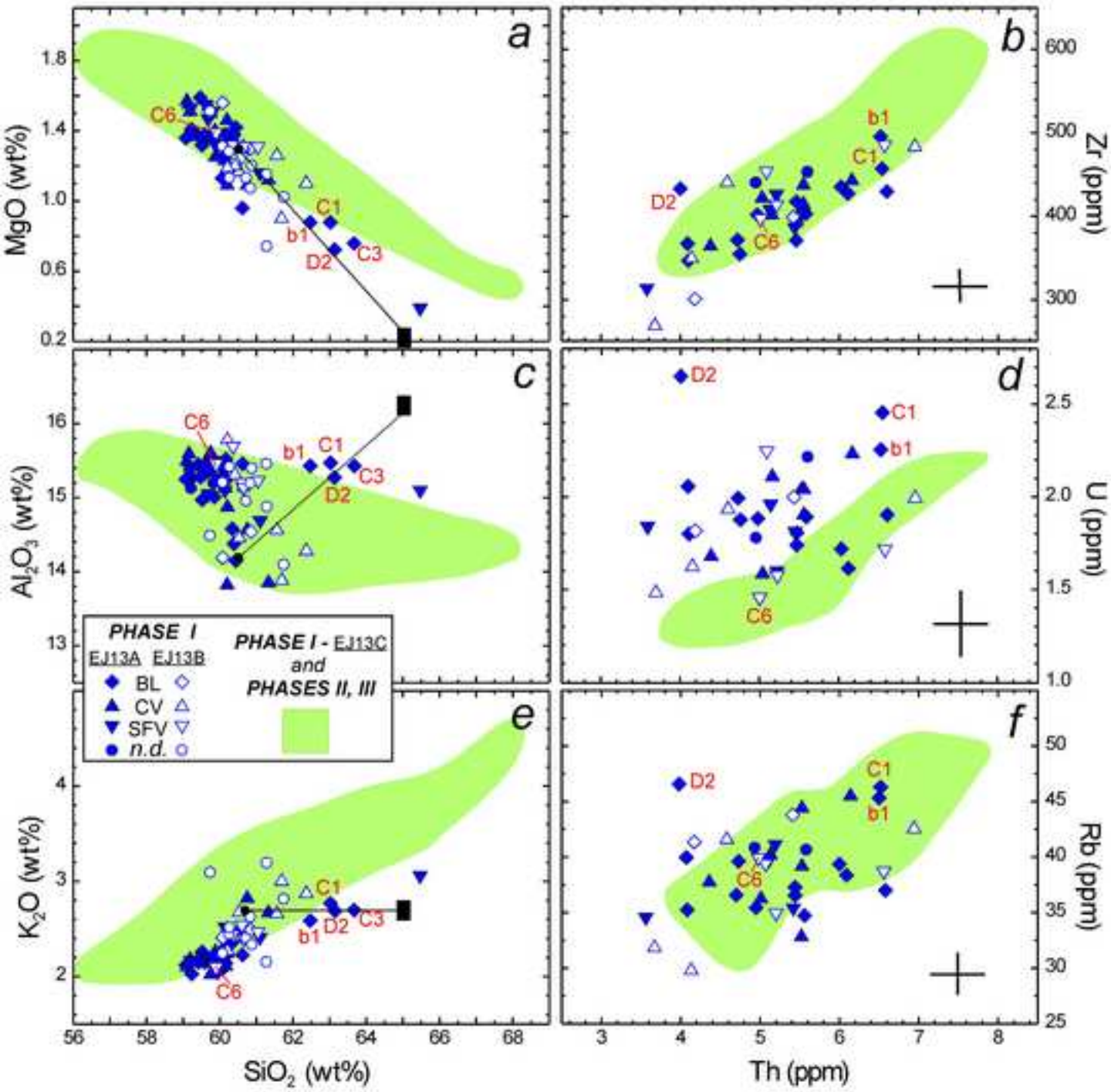

Figure 5

Click here to download high resolution image

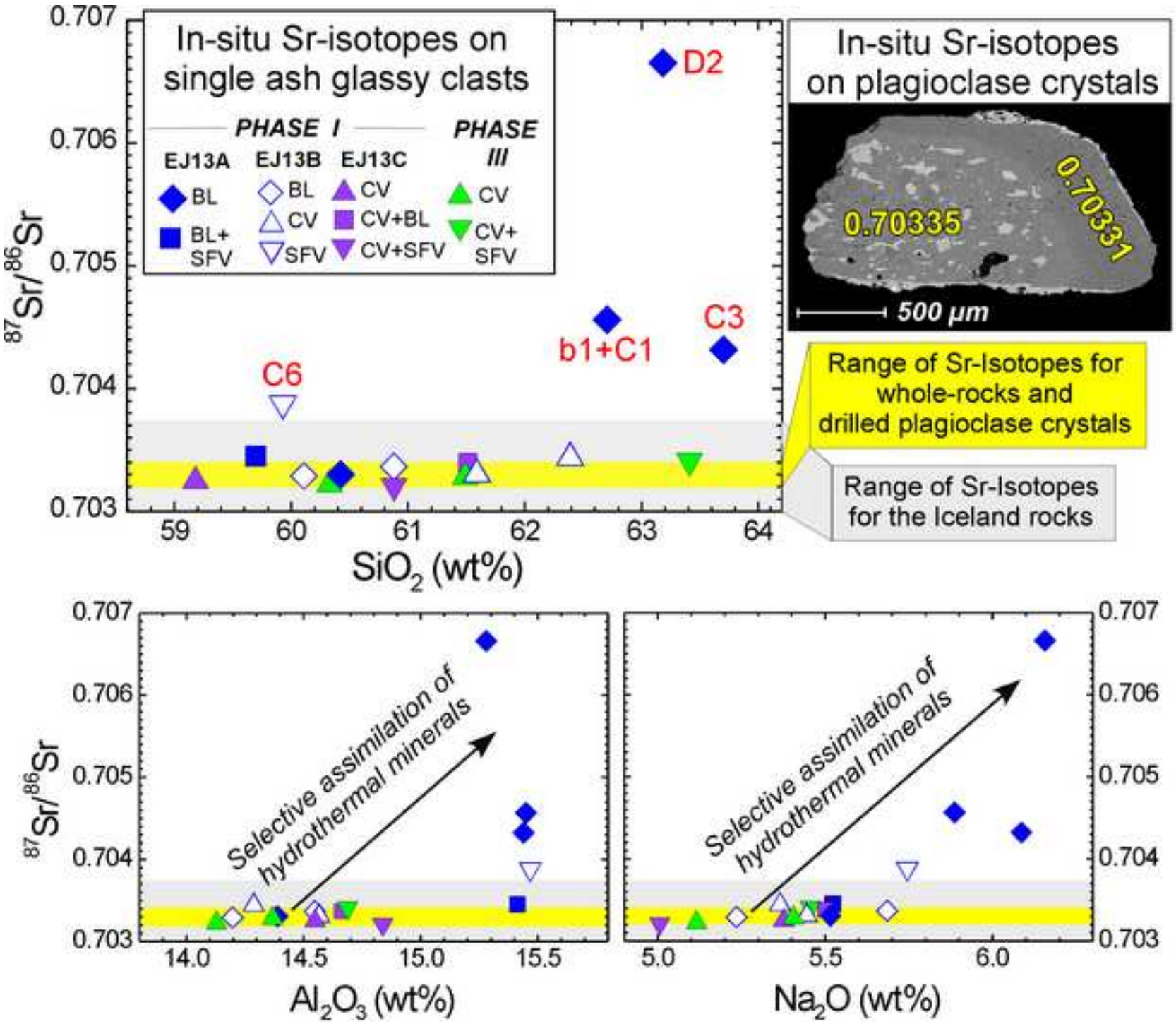

Figure 6

Click here to download high resolution image

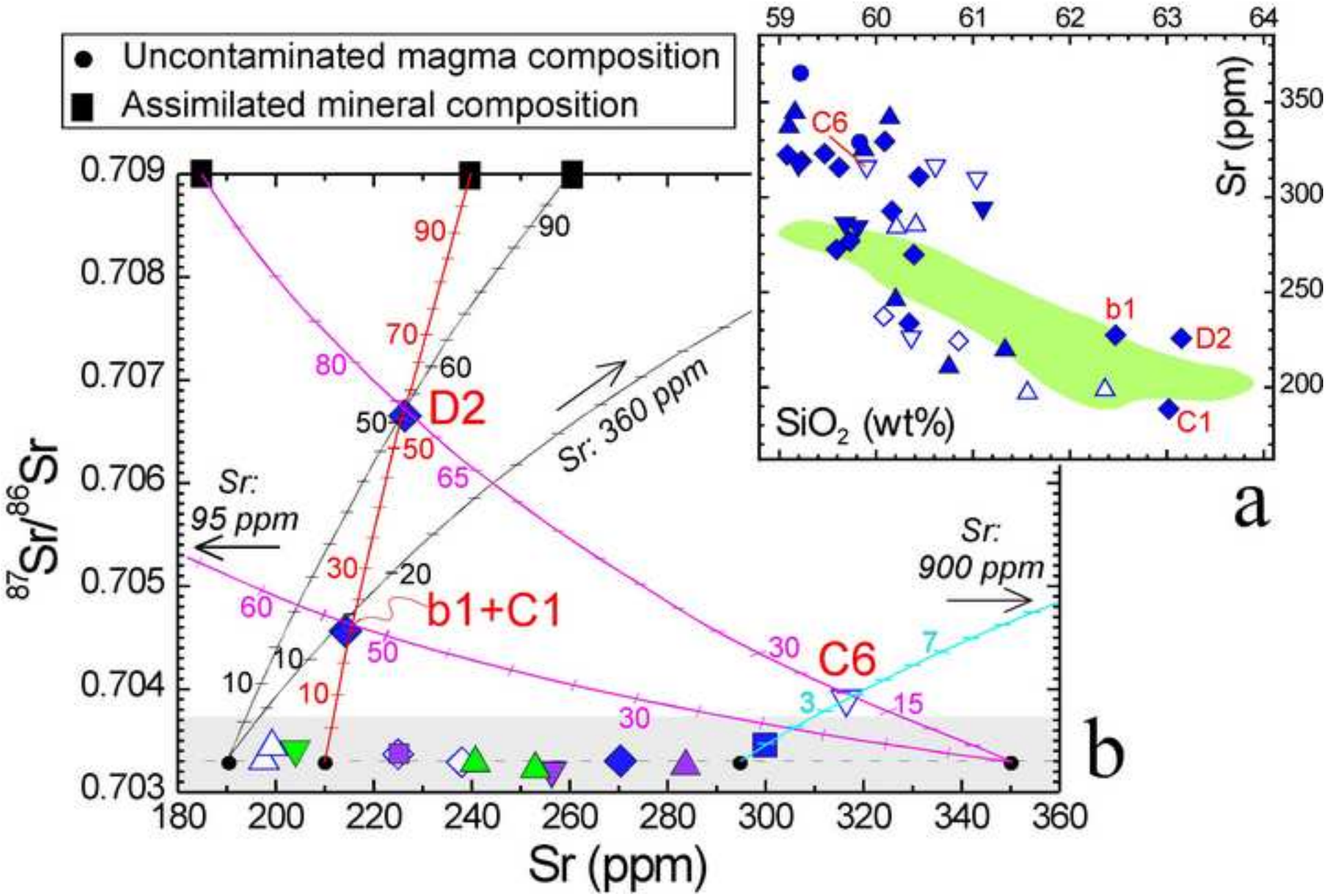

Figure 7

Click here to download high resolution image